Illumination-based normalization for wave-equation depth migration

James E. Rickett

ChevronTexaco Exploration and Production Technology Company,

6001 Bollinger Canyon Road, San Ramon, CA 94583-2324

formerly Stanford Exploration Project, Department of Geophysics,

Stanford University, Stanford, CA 94305-2215

Manuscript on October 25, 2001[1]

ABSTRACT

Illumination problems caused by finite-recording aperture and lateral velocity lensing can lead to biased amplitudes in migrated seismic images. I calculate weighting functions that compensate for illumination problems in wave-equation depth migration. The methodology takes into account reflector dip as well as both shot and receiver geometries, and because it is based on wave-equation migration, it naturally models the finite-frequency effects of wave propagation. The first step in the process is to model synthetic data with the true recording geometry over a reference model. Migrating the synthetic data then produces an image whose amplitude can be compared to the reference image to produce an illumination-based weighting function. These weighting functions can be applied directly to the migrated images to mitigate the effects of poor subsurface illumination. The reference model should be as close to the true model as possible; good choices include the migrated image, or a synthetic image with a single known dip that corresponds to the expected dip of a reflector of

[1]This paper was presented at the 71st Annual International Meeting of the Society of Exploration Geophysicists in San Antonio, 2001.

interest. Computational shortcuts allow the weighting functions to be computed at about the cost of a single migration. Results indicate that model-space normalization can significantly reduce amplitude distortions due to irregular subsurface illumination.

INTRODUCTION

Seismic migration algorithms based directly on solutions to a finite-frequency acoustic wave equation are often referred to as "wave-equation" migration methods. This is in contrast to Kirchhoff-integral methods that usually depend on high-frequency asymptotic (ray) approximations. Wave-equation methods have the advantage over Kirchhoff algorithms in that they naturally model the finite-frequency effects of wave propagation such as multi-pathing. These phenomena often cause problems in structurally complex areas, and require special treatment with ray-based imaging algorithms.

For robustness, wave-equation migration algorithms are often formulated as the adjoint of a linear forward modeling operator rather than the inverse [e.g. Claerbout (1995)]. This means that, although migration treats kinematics correctly, the amplitudes of migrated images do not accurately represent seismic reflectivity.

Wave-equation migration can be also be formulated as an inverse operation, so that the imaging procedure preserves reflector amplitudes. Necessary components of amplitude-preserving imaging include honoring the physics of wave-propagation in the extrapolation operator, and careful choice of imaging condition. Stolt and Benson (1986) describe how to the model the amplitude affects of wave-propagation in $v(z)$ media with WKBJ Green's functions, and how to preserve amplitude at the imaging step. Sava et al. (2001) extend the true-amplitude imaging condition of shot-geophone (DSR) migration for imaging reflectivity as a function of incidence angle.

In media with lateral velocity variations, however, another important phenomena comes into play: lateral focusing and defocusing of the seismic wavefield. Even if the wavefield is regularly sampled on the surface, illumination below a complex salt structure may be sparse and irregular (Muerdter et al., 1996; Wyatt et al., 1997; Bear et al., 1999). Even U/D shot-profile imaging conditions (Claerbout, 1971) based on deconvolving the downward-going source wavefield (D) from the upward-going receiver wavefield (U) do not take into account limitations in the recording geometry that can also affect subsurface illumination.

An alternative approach to migration/inversion is to leverage the power of geophysical inverse theory (Tarantola, 1987); this provides a rigorous framework for estimating earth models that are consistent with some observed set of data. Least-squares ($L2$) migration follows this philosophy [see Ronen and Liner (2000) for a review], and has the potential to accurately image amplitudes, even in areas of irregular illumination. Nemeth et al. (1999) and Duquet et al. (2000) describe the application of least-squares Kirchhoff migration, and more recently Prucha et al. (2000) and Kuehl and Sacchi (2001) formulate shot-geophone (DSR) migration as a least-squares problem. As with many other industrial-scale geophysical inverse problems, the matrices involved in $L2$ depth migration are too large to invert directly, and we depend on iterative gradient-based linear solvers to estimate solutions. However, operators such as prestack depth migration are so expensive to apply that we can only afford to iterate a handful of times, at best. Another major problem with $L2$ migration is its sensitivity to the details of the implementation; the choice of inversion parameters, such as the amount and style of regularization, can significantly impact the inversion results.

In this paper, I describe an approximate solution to the problem of irregular illumination in wave-equation migration. The method involves modeling synthetic data over a reference model, migrating the synthetic data, and creating an illumination-based weighting function from on the ratio between the reference model and the modeled and remigrated reference model. As well as providing infor-

mation about subsurface illumination, this weighting function can then be applied to the migrated image to compensate for the effects of irregular illumination. Furthermore, because the weighting functions are derived from wave-equation migration, they model the finite-frequency nature of wave propagation in complex media; in contrast to ray-based illumination, there is no need to smooth either the velocity model to stabilize a ray-tracing algorithm, or the illumination functions over an effective Fresnel zone (Schneider and Winbow, 1999).

THEORY

The canonical geophysical inverse problem can be summarized as follows: given a linear forward modeling operator $\mathbf{A}$, and some recorded data $\mathbf{d}$, estimate a model $\mathbf{m}$ such that $\mathbf{A}\mathbf{m} \approx \mathbf{d}$. If the system is over-determined, the model that minimizes the expected error in predicted data is given by:

$$\mathbf{m}_{L2} = (\mathbf{A}'\mathbf{A})^{-1}\,\mathbf{A}'\mathbf{d}. \tag{1}$$

Because of the high cost of each iteration of a gradient-based solver with expensive depth migration operators, the successful application of $L2$ depth migration may depend on strategies employed to speed convergence.

To reduce the number of solver iterations required to reach a satisfactory result, we can always change model-space variables from $\mathbf{m}$ to $\mathbf{x}$ through a linear operator $\mathbf{P}$, and solve the following new system for $\mathbf{x}$,

$$\mathbf{B}'\mathbf{d} = \mathbf{B}'\mathbf{B}\mathbf{x}, \tag{2}$$

where $\mathbf{B} = \mathbf{A}\mathbf{P}$. When we find a solution, we can then recover the model estimate, $\mathbf{m}_{L2} = \mathbf{P}\mathbf{x}$. If we choose the operator $\mathbf{P}$ such that $\mathbf{B}'\mathbf{B} \approx \mathbf{I}$, then the adjoint solution, given by

$$\hat{\mathbf{m}} = \mathbf{P}\mathbf{B}'\mathbf{d} = \mathbf{P}\mathbf{P}'\mathbf{A}'\mathbf{d}, \tag{3}$$

will yield a good model estimate; furthermore, gradient-based solvers should converge to a solution of the new system rapidly in only a few iterations. The problem then becomes: what is a good choice of preconditioning operator **P**?

Rather than trying to solve the full inverse problem given by equation (1), in this paper I look for adjoint solutions of the same form as equation (3). However, rather looking for dense preconditioning operators, I restrict the search to real diagonal weighting functions $\mathbf{W}_\mathrm{m}$, so that equation (3) becomes

$$\hat{\mathbf{m}} = \mathbf{W}_\mathrm{m}^2 \, \mathbf{A}' \mathbf{d} \approx \mathbf{m}_{L2}. \tag{4}$$

$\mathbf{W}_\mathrm{m}$ can be applied to the migrated (adjoint) image with equation (4); however, in their review of $L2$ migration, Ronen and Liner (2000) observe that normalized migration is only a good substitute for full (iterative) $L2$ migration in areas of high signal-to-noise. In these cases, $\mathbf{W}_\mathrm{m}$ could be used as a model-space preconditioner to the full $L2$ problem, as described above.

Claerbout and Nichols (1994) noticed that if we model and remigrate a reference image, the ratio between the reference image and the modeled/remigrated image will be a weighting function with the correct physical units. Following the notation that $\mathbf{diag}(\mathbf{m}_\mathrm{ref})$ refers to a matrix created by spreading the elements of the vector $\mathbf{m}_\mathrm{ref}$ along its diagonal, the weighting function $\mathbf{W}_\mathrm{m}$, whose square is given by

$$\mathbf{W}_\mathrm{m}^2 = \frac{\mathbf{diag}(\mathbf{m}_\mathrm{ref})}{\mathbf{diag}(\mathbf{A}' \mathbf{A} \, \mathbf{m}_\mathrm{ref})} \approx \left(\mathbf{A}' \mathbf{A}\right)^{-1}, \tag{5}$$

will have the same units as $\mathbf{A}^{-1}$. Furthermore, $\mathbf{W}_\mathrm{m}^2$ will be the *ideal* weighting function if the reference model equals the true model and the modeling/migration operator correctly mimics the physics of the system.

Equation (5) and its application to wave-equation depth migration forms the basis for the first part of this paper. However, when following this approach, there are two important practical considerations to take into account: firstly, the choice of reference image, and secondly, the problem of

dealing with zeros in the denominator.

Although equation (5) is valid for general linear operators, and including both shot-geophone migration with the double square root equation, and shot-profile migration with the single square root equation

For the examples in this paper, I implement $\mathbf{A}'$ as shot-profile migration with a Fourier finite-difference (FFD) one-way extrapolator (Ristow and Ruhl, 1994). FFD combines the steep-dip accuracy of phase-shift migration with the strength of finite-differences in areas of strong lateral velocity gradients. The adjoint of the migration, describes shot-profile modeling; this is implemented by downward-continuing the source wavefield into the earth, then recursively upward-continuing the scattered field, convolving in contributions from the source wavefield based on local reflectivity. I constructed the amplitude response of the modeling and migration operators to be pseudo-unitary rather than amplitude-preserving, and they pass the dot-product test (Claerbout, 1995) indicating they describe true adjoint processes.

Similar normalization schemes [e.g. Slawson et al. (1995); Chemingui (1999); Duquet et al. (2000)] have been proposed for Kirchhoff migration operators. In fact, both Nemeth et al. (1999) and Duquet et al. (2000) report success with using diagonal model-space weighting functions as preconditioners for Kirchhoff $L2$ migrations. However, normalization schemes that work for Kirchhoff migrations are not computationally feasible for recursive migration algorithms based on downward-continuation.

Various authors (O'Brien and Etgen, 1998; Rickett, 2001; Zhou and Stein, 2001) have calculated illumination functions for wave-equation migration based on integrating the downward-propagating shot energy. This approach fails to take into account limitations in the receiver geometry, and is only appropriate if the upward-propagating wavefield is fully sampled (Rickett, 2001). Shin et al. (2001)

described a clever algorithm for calculating the diagonal elements of the Hessian matrix ($\mathbf{A}'\mathbf{A}$) for reverse-time shot-profile migration, and its application for describing wavefield illumination. In contrast to the methods presented here, however, the main diagonal itself does not capture the sensitivity of illumination to the local reflector dip (Rickett, 2001; Biondi, 2001).

Three choices of reference image

The ideal reference image would be the true subsurface model. However, since we do not know what that is, we have to substitute an alternative model. In the numerical examples section below, I experiment with three practical alternatives, which I will denote $\mathbf{m}_1$, $\mathbf{m}_2$, and $\mathbf{m}_3$.

Claerbout and Nichols (1994) attribute to Symes the idea of using the adjoint (migrated) image as the reference model. The rationale for this is that migration provides a robust estimate of the true model. As the first alternative I follow this suggestion, so that $\mathbf{m}_1 = \mathbf{A}'\mathbf{d}$. A second alternative is to try an reference image of purely random numbers: $\mathbf{m}_2 = \mathbf{r}$, where $\mathbf{r}$ is a random vector. This is has the advantages that it contains a variety of dips, and is not influenced by the data. However, it has the disadvantage that different realizations of $\mathbf{r}$ may produce different weighting functions. The third alternative that I discuss ($\mathbf{m}_3$) is a monochromatic reference image, consisting of purely flat events. This approach can be described as "flat-event calibration", and closely follows the methodology Black and Schleicher (1989) proposed for normalizing dip moveout (DMO) in the presence of irregular acquisition geometry.

Stabilizing the denominator

To avoid division by zero, Claerbout and Nichols (1994) suggest multiplying both the numerator and denominator in equation (5) by $\mathbf{diag}(\mathbf{A}'\mathbf{A}\,\mathbf{m}_{\text{ref}})$, and stabilizing the division by adding a small positive

number to the denominator:

$$\mathbf{W}_{\mathrm{m}}^2 = \frac{\mathbf{diag}(\mathbf{m}_{\mathrm{ref}}) \cdot \mathbf{diag}(\mathbf{A}' \mathbf{A}\, \mathbf{m}_{\mathrm{ref}})}{|\mathbf{diag}(\mathbf{A}' \mathbf{A}\, \mathbf{m}_{\mathrm{ref}})|^2 + \epsilon^2 \mathbf{I}}, \tag{6}$$

Although this does solve the problem of division by zero, the numerator and denominator will still oscillate rapidly in amplitude with the phase of the image.

Illumination, however, should be independent of the wavefield's phase. Therefore, I calculate weighting functions from the ratio of the smoothed analytic signal envelopes (denoted by $<>$) of the model-space images:

$$\mathbf{W}_{\mathrm{m}}^2 = \frac{\mathbf{diag}(< \mathbf{m}_{\mathrm{ref}} >)}{\mathbf{diag}(< \mathbf{A}' \mathbf{A}\, \mathbf{m}_{\mathrm{ref}} >) + \epsilon^2 \mathbf{I}}, \tag{7}$$

where ϵ is a damping parameter that is related to the signal-to-noise level.

NUMERICAL EXAMPLES

The Amoco 2.5-D synthetic dataset (Etgen and Regone, 1998) provides an excellent test for the weighting functions discussed above. The velocity model (Figure 1) contains significant structural complexity in the upper 3.8 km, and a flat reflector of uniform amplitude at about 3.9 km depth. Since the entire velocity model ("Canadian foothills overthrusting onto the North Sea") is somewhat pathological, I restricted my experiments to the North Sea section of the dataset ($x > 11$ km).

The data were generated by 3-D acoustic finite-difference modeling of the 2.5-D velocity model. However, making the test more difficult is the fact that the 2-D linear one-way FFD extrapolators (Ristow and Ruhl, 1994), which I use for modeling and migration, do not accurately predict the 3-D geometric spreading and multiple reflections that are present in this dataset. This is illustrated in Figure 2, which compares equivalent shot gathers modeled by the different algorithms; although their kinematics are very close, their amplitudes differ significantly.

Figure 3 compares the shot-profile migration image ($\mathbf{m}_1$) with the results of remodeling and remigrating the three reference images as described above. A direct comparison between panels 3 (a) and (b) indicates that the modeling and remigration process further decreases amplitudes in areas of poor illumination, both beneath the salt and on the steeply dipping salt flanks. Furthermore, the effect of irregular illumination, both from the limited acquisition geometry on the surface, and focusing by the lateral velocity contrasts, is clearly visible on the three remigrations in panels 3 (b-d).

Figure 4 compares the illumination calculated from the three reference images with the raw shot illumination, calculated by integrating the downward-going shot energy. Noticeably, the shot-only weighting function [panel (a)] does not take into account the off-end (as opposed to split-spread) receiver geometry. Panel (b), the weighting function derived from model $\mathbf{m}_1$, appears slightly noisy. However, in well-imaged areas (e.g. along the target reflector), the weighting function is well-behaved. Panel (c) shows the weighting function derived from the random reference image ($\mathbf{m}_2$). Despite the smoothing, this weighting function clearly bears the stamp of the random number field. A feature of white noise is that no amount of smoothing will be able to remove the imprint of the random numbers completely. The final panel (d) shows the flat-event illumination weighting function, derived from $\mathbf{m}_3$. This is noise-free and very well-behaved since it depends only on the velocity model and recording geometry, not the data. However, it only represents the true illumination for flat reflectors.

The image in Figure 5 has been normalized with the weighting function derived from the the migrated-image reference model ($\mathbf{m}_1$). The basement reflector is more continuous than in Figure 3 (a), and the effect of the recording geometry is less pronounced. Although not shown here, similar features are also visible on the other normalized images.

For a quantitative comparison between normalized migration results, I picked the maximum am-

Weighting function:	NSD:
No weighting function	0.229
Shot illumination	0.251
$\mathbf{m}_{\text{ref}} = \mathbf{m}_1$ (migrated image)	0.148
$\mathbf{m}_{\text{ref}} = \mathbf{m}_2$ (random image)	0.195
$\mathbf{m}_{\text{ref}} = \mathbf{m}_3$ (flat events)	0.140

Table 1.

plitude of the 3.9 s reflection event on the calibrated images. The normalized standard deviation (NSD) of these amplitudes is shown in Table 1, where

$$\text{NSD} = \sqrt{\sum_{i_x} \left(\frac{a_{i_x}}{\overline{a}} - 1 \right)^2}. \tag{8}$$

Table 1, therefore, provides a measure of how well the various weighting function compensate for illumination difficulties. The picked-basement amplitudes of the raw migration, and the migration after flat-event normalization are shown in Figure 6. This graphically illustrates that for this model the normalization procedure improves amplitude reliability by almost a factor of two.

To compare the normalized migration results with those produced by full $L2$ shot-profile Fourier finite-difference migration, I ran ten iterations of full conjugate gradients, using an out-of-core optimization library (Sava, 2001). Figure 7 shows the migrated images produced after four and ten iterations. As the inversion proceeds, it does begin to compensate for irregular illumination. However, I did not impose an explicit regularization term during the inversion; therefore, as the solution evolves, other poorly-constrained components of the model-space start to appear in the solution, including both low and high frequency noise, steeply-dipping energy, and multiple energy that is not modeled by the linear forward modeling operator. The increase in noise causes the NSD to actually

begin to increase after the fourth iteration (see Figure 8), implying a decrease in image quality.

DISCUSSION

Computational cost

As it stands, the cost of computing a weighting function of this kind is twice the cost of a single migration. Add the cost of the migration itself, and this approach is 25% cheaper than running two iterations of conjugate gradients, which costs two migrations per iteration.

However, the bandwidth of the weighting functions is much lower than that of the migrated images. This allows considerable computational savings, as modeling and remigrating a narrow frequency band around the central frequency produces similar weighting functions than the full bandwidth. Repeating the first experiment ($\mathbf{m}_{\text{ref}} = \mathbf{m}_1$) with half the frequencies gives a NSD $= 0.147$, which is almost as good as before at half the cost.

Range of validity

The methodology described in this paper is valid for any linear operator; although my implementation was shot-profile modeling with a one-way extrapolator, the principles are equally applicable to other wave-equation migration algorithms such as shot-geophone (double square root) migration.

As with any deconvolution or inversion, however, there are potential pitfalls. Most importantly, the forward modeling operator must model the physics of the system sufficiently accurately; this includes both the physics of wave propagation, and the true earth velocity. In practice, earth velocity models are never completely true-to-life. Furthermore, linear forward modeling does not predict multiple scattering, and so multiple energy needs to be removed as a preprocessing step, prior to

migration.

CONCLUSION

Model-space weighting functions based on equation (7) provide a robust way to compensate for illumination problems during wave-equation depth migration based on downward-continuation. Illumination functions calculated in this way have the advantage over ray-based illumination functions in that the they accurately model the finite-frequency nature of wave propagation, and there is no need for smoothing of either the velocity model or the illumination function.

The choice of reference image is important, and results here suggest either the migrated image, or an image consisting of the expected dip of the reflector of interest, may be appropriate choices. Additionally, computational shortcuts allow the cost of the normalized migration to be reduced to only about twice the cost of a standard migration.

ACKNOWLEDGEMENTS

I would like to thank the sponsors of the Stanford Exploration Project for providing the financial assistance for this work, and BP for releasing this dataset to Stanford.

REFERENCES

Bear, G., Lu, R., Lu, C.-P., Watson, I., and Willen, D., 1999, The construction of subsurface illumination and amplitude maps via ray-tracing: 69th Annual Internat. Mtg., Soc. Expl. Geophys., Expanded Abstracts, 1532–1535.

Biondi, B. L., 2001, 3-D seismic imaging: Stanford Exploration Project, lecture notes available at http://sepwww.stanford.edu/sep/biondo/research.html.

Black, J. L., and Schleicher, K., 1989, Effect of irregular sampling on prestack DMO: 59th Annual Internat. Mtg., Soc. Expl. Geophys., Expanded Abstracts, 1144–1147.

Chemingui, N., 1999, Imaging irregularly sampled 3D prestack data: Ph.D. thesis, Stanford University.

Claerbout, J., and Nichols, D., 1994, Spectral preconditioning: Stanford Exploration Project Report, **82**, 183–186.

Claerbout, J. F., 1971, Toward a unified theory of reflector mapping: Geophysics, **36**, no. 3, 467–481.

Claerbout, J. F., 1995, Basic earth imaging: Stanford Exploration Project.

Duquet, B., Marfurt, K. J., and Dellinger, J. A., 2000, Kirchhoff modeling, inversion for reflectivity, and subsurface illumination: Geophysics, **65**, no. 4, 1195–1209.

Etgen, J., and Regone, C., 1998, Strike shooting, dip shooting, widepatch shooting — Does prestack depth migration care? A model study: 68th Annual Internat. Mtg., Soc. Expl. Geophys., Expanded Abstracts, 66–69.

Kuehl, H., and Sacchi, M. D., 2001, Generalized least-squares DSR migration using a common angle imaging condition: 71st Annual Internat. Mtg., Soc. Expl. Geophys., Expanded Abstracts, 1025–1028.

Muerdter, D. R., Lindsay, R. O., and Ratcliff, D. W., 1996, Imaging under edges of salt sheets: A raytracing study: 66th Annual Internat. Mtg., Soc. Expl. Geophys., Expanded Abstracts, 578–580.

Nemeth, T., Wu, C., and Schuster, G. T., 1999, Least-squares migration of incomplete reflection data: Geophysics, **64**, no. 1, 208–221.

O'Brien, M. J., and Etgen, J. T., 1998, Wavefield imaging of complex structures with sparse point-receiver data: 68th Annual Internat. Mtg., Soc. Expl. Geophys., Expanded Abstracts, 1365–1368.

Prucha, M. L., Clapp, R. G., and Biondi, B., 2000, Seismic image regularization in the reflection angle domain: Stanford Exploration Project Report, **103**, 109–119.

Rickett, J. E., 2001, Spectral factorization of wavefields and wave operators: Ph.D. thesis, Stanford University.

Ristow, D., and Ruhl, T., 1994, Fourier finite-difference migration: Geophysics, **59**, no. 12, 1882–1893.

Ronen, S., and Liner, C. L., 2000, Least-squares DMO and migration: Geophysics, **65**, no. 5, 1364–1371.

Sava, P., Fomel, S., and Biondi, B., 2001, Amplitude-preserved common-image gathers by wave-equation migration: 71st Annual Internat. Mtg., Soc. Expl. Geophys., Expanded Abstracts, 296–299.

Sava, P., 2001, An out-of-core optimization library: Stanford Exploration Project Report, **108**, 199–224.

SchneiderJr., W., and Winbow, G., 1999, Efficient and accurate modeling of 3-D seismic illumination: 69th Annual Internat. Mtg., Soc. Expl. Geophys., Expanded Abstracts, 633–636.

Shin, C., Jang, S., and Min, D.-J., 2001, Improved amplitude preservation for prestack depth migration by inverse scattering theory: Geophysical Prospecting, **49**, no. 5, 592–606.

Slawson, S. E., Monk, D. J., and Sudhakar, V., 1995, DMO implications for 3-D survey design: 65th Annual Internat. Mtg., Soc. Expl. Geophys., Expanded Abstracts, 935–938.

Stolt, R. H., and Benson, A. K., 1986, Seismic migration: Geophysical Press, London.

Tarantola, A., 1987, Inverse problem theory: Elsevier Science Publ. Co., Inc., Amsterdam.

Wyatt, K. D., Valasek, P. A., Wyatt, S. B., and Heaton, R. M., 1997, Velocity and illumination from horizon-based PSDM: 67th Annual Internat. Mtg., Soc. Expl. Geophys., Expanded Abstracts, 1801–1804.

Zhou, Z.-Z., and Stein, J. A., 2001, Practical, accurate, full-azimuth 3-D prestack finite difference depth migration: 71st Annual Internat. Mtg., Soc. Expl. Geophys., Expanded Abstracts, 949–952.

LIST OF FIGURES

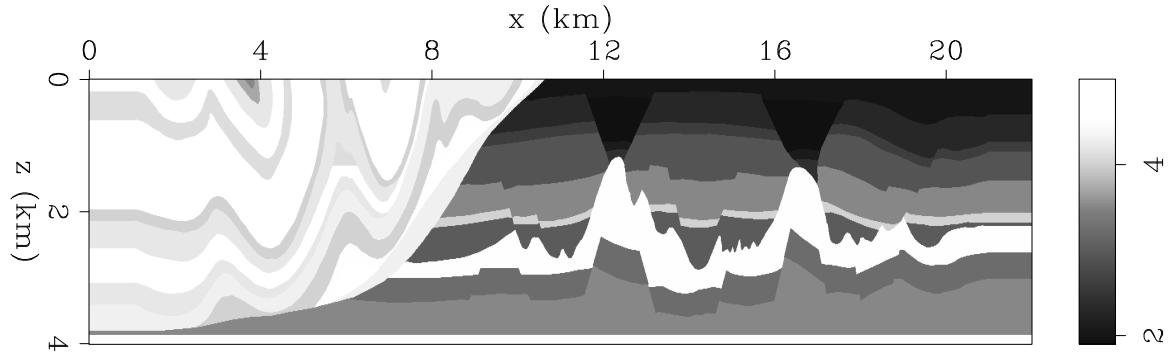

Figure 1.

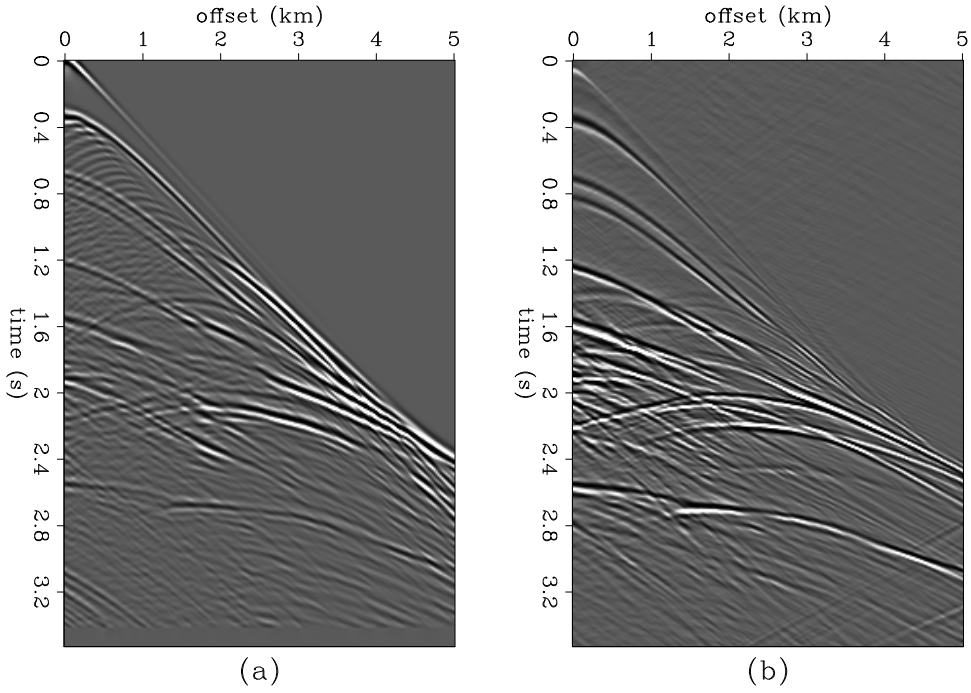

Figure 2.

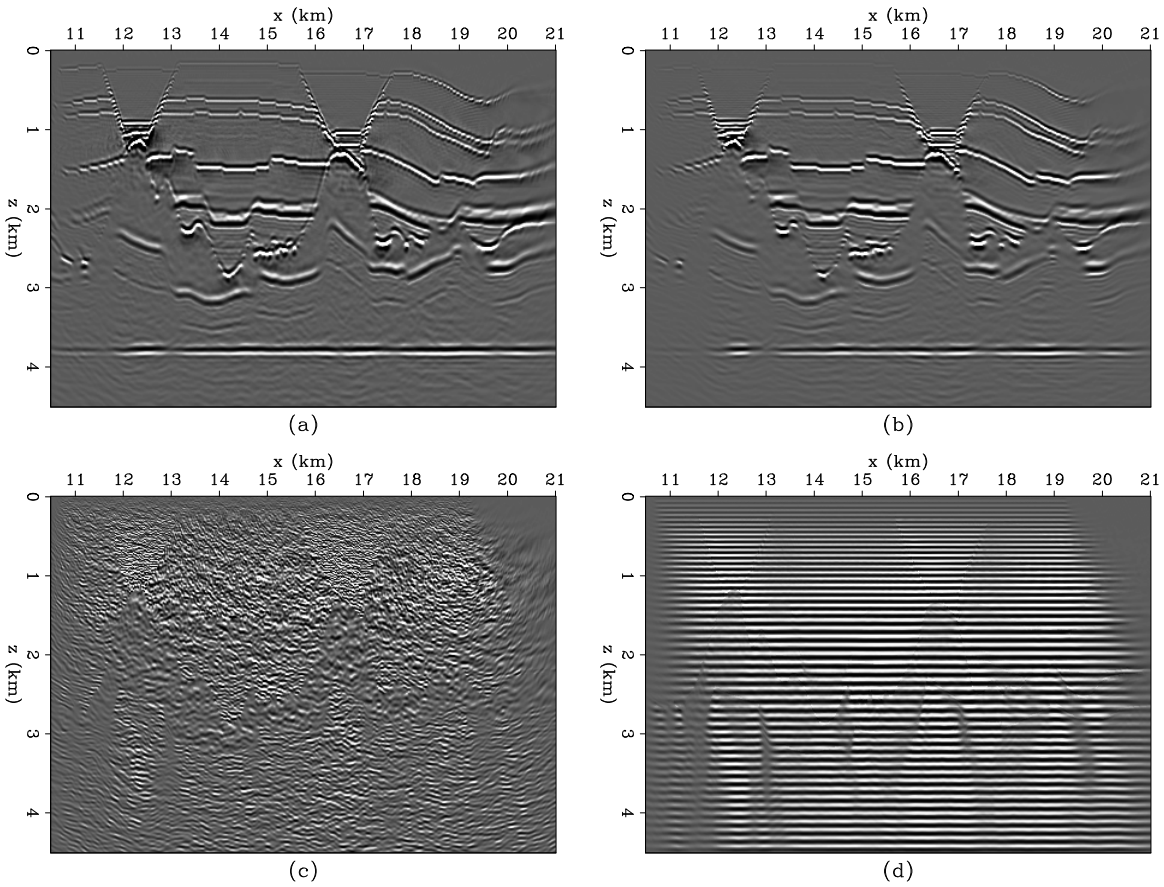

Figure 3.

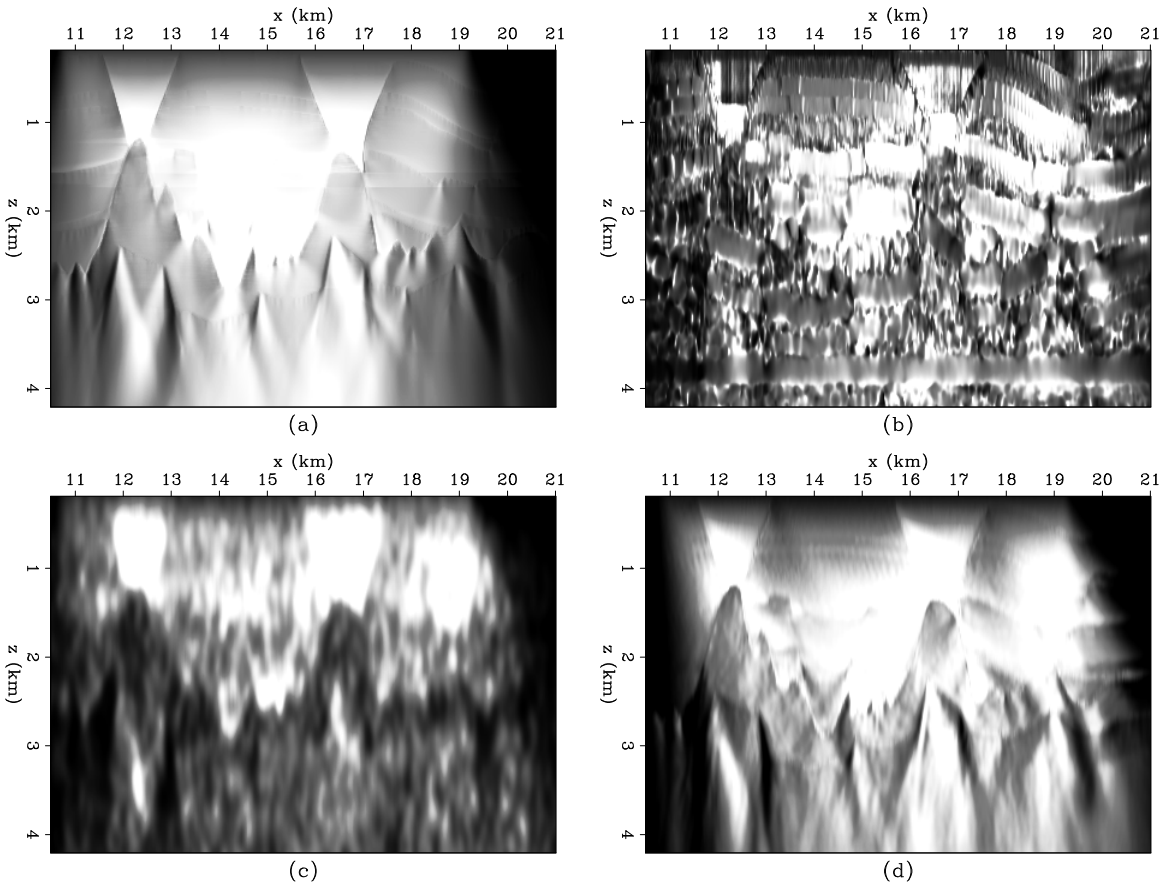

Figure 4.

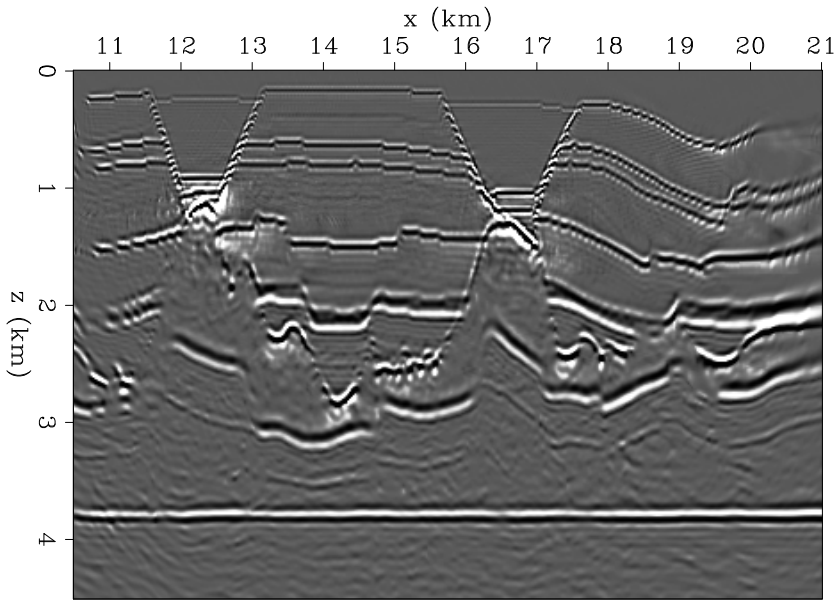

Figure 5.

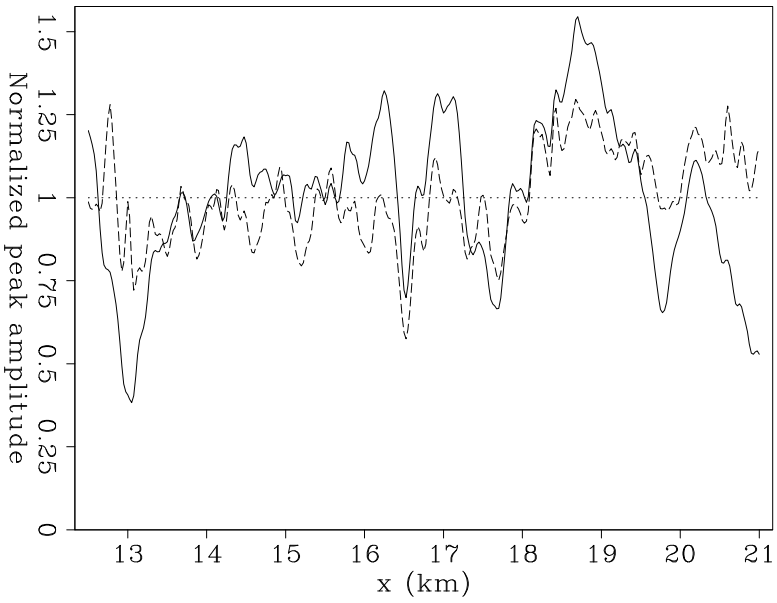
Normalized peak amplitude
0
0.25
0.5
0.75
1
1.25
1.5
13
14
15
16
17
18
19
20
21
x (km)

Figure 6.

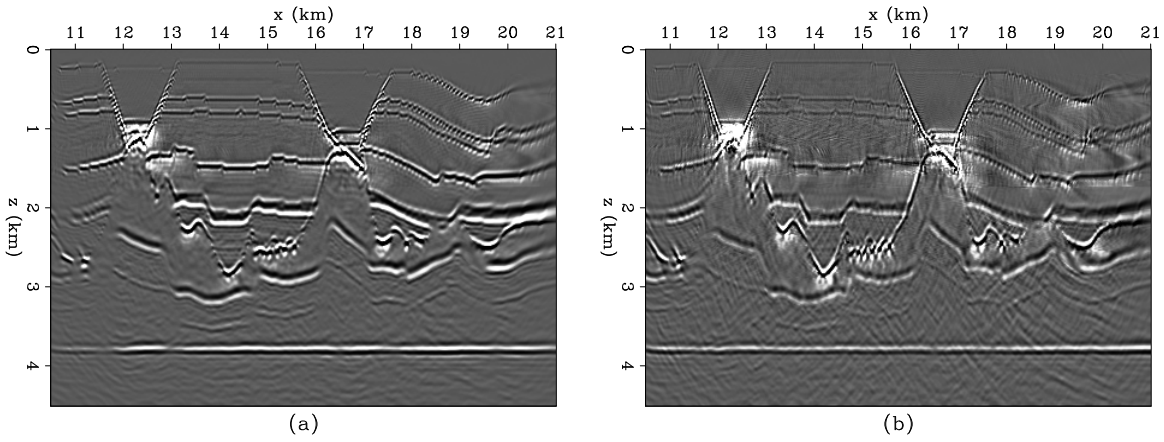
x (km)
11 12 13 14 15 16 17 18 19 20 21
0 1 2 3 4
z (km)
(a)
x (km)
11 12 13 14 15 16 17 18 19 20 21
0 1 2 3 4
z (km)
(b)

Figure 7.

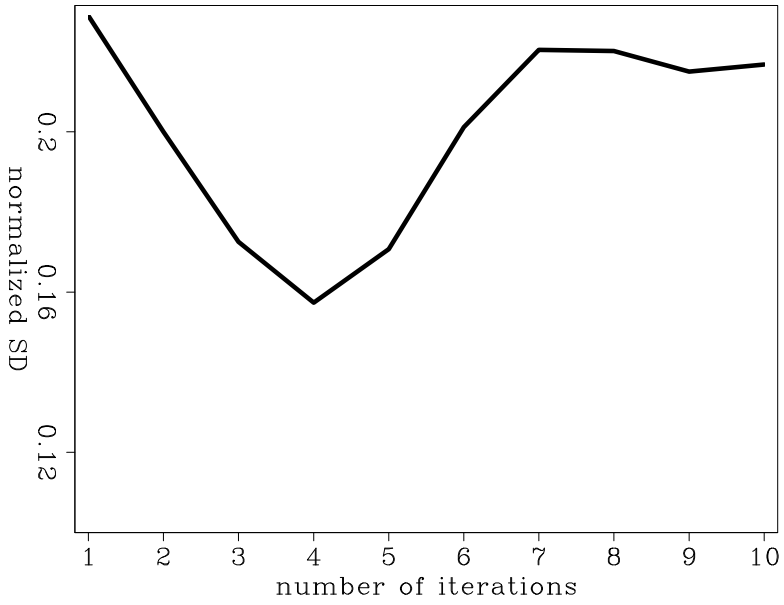

Figure 8.